JOURNAL OF APPLIED PHYSICS **109**, 084526 (2011)

Dynamics of explosively imploded pressurized tubes

Daniel Szirti,[1,a)] Jason Loiseau,[1] Andrew Higgins,[1] and Vincent Tanguay[2]
[1]*Department of Mechanical Engineering, McGill University, Montreal H3A 2K6, Canada*
[2]*Defence Research and Development Canada Valcartier, Quebec, Quebec G3J 1X5, Canada*

(Received 21 November 2010; accepted 17 February 2011; published online 29 April 2011)

The detonation of an explosive layer surrounding a pressurized thin-walled tube causes the formation of a virtual piston that drives a precursor shock wave ahead of the detonation, generating very high temperatures and pressures in the gas contained within the tube. Such a device can be used as the driver for a high energy density shock tube or hypervelocity gas gun. The dynamics of the precursor shock wave were investigated for different tube sizes and initial fill pressures. Shock velocity and standoff distance were found to decrease with increasing fill pressure, mainly due to radial expansion of the tube. Adding a tamper can reduce this effect, but may increase jetting. A simple analytical model based on acoustic wave interactions was developed to calculate pump tube expansion and the resulting effect on the shock velocity and standoff distance. Results from this model agree quite well with experimental data. © *2011 American Institute of Physics*. [doi:10.1063/1.3567919]

I. INTRODUCTION

The high energy and power densities of high explosives make them desirable drivers for hypervelocity launchers and shock tubes capable of achieving extremely high temperatures and pressures. The ability of the energy release of explosives to be focused inward (i.e., implosion) permits that energy to be concentrated to an almost arbitrarily high degree. A well-known example is the shaped charge effect, in which a metal-lined conical cavity is imploded by the detonation of explosive surrounding the cavity, resulting in some of the metal liner being ejected forward in a thin jet which travels faster than the velocity of detonation (VOD) of the explosive used. Specially designed shaped charges with cylindrical cavities have demonstrated incoherent jets at velocities as great as 70 km/s or faster.[1]

In order to retain the integrity of a solid projectile launched using an explosive-driven hypervelocity launcher, or to design a shock tube with a uniform, well-quantified post-shock state, it is desirable to have a continuously driven linear implosion. For example, while a hypervelocity launcher in which a spherically imploding wave is focused onto a projectile can, in theory, generate projectile velocities in excess of 10 km/s, in practice, the projectile is unable to survive the intense loading at the focus point of the implosion.[2] Alternatively, if the implosion process is distributed continuously along the launch tube, the projectile loading can be maintained at a nearly constant moderate level for the entire launch cycle (note that "moderate" may still mean accelerations as great as 10^8 m/s^2).

A hypervelocity launcher using a linear implosion along the length of the launcher was developed in the 1960s by Physics International (PI) under funding from National Aeronautics and Space Administration (NASA) for the purpose of simulating micrometeoroid impacts in the laboratory.[3–7] In this device, the linearly imploded tube served the same role as a pump tube in a conventional two-stage light gas gun, with the explosive pinch of a helium-pressurized tube acting as a mechanical piston to dynamically compress the helium, which was used as the driver gas in a conventional gas gun cycle. See Fig. 1 for a sketch demonstrating the operation of the linearly imploded pump tube, or driver, section of the launcher. The virtual piston formed by the explosive pinch travels down the tube at the VOD of the explosive and drives a strong precursor shock wave (PSW) in the driver gas in front of it. Menikoff *et al.*[8] demonstrated both analytically and experimentally with smear photography and flash x-ray that the shock reaches planarity very early on; Crosby and Gill[4] also obtained photographic evidence of the planarity of the shock using a framing camera. Advanced implementations of the PI launcher concept had the explosive continue onto the reservoir section of the launcher and along the launch tube, where the explosive pinch maintained high pressure helium on the base of the projectile. The use of an explosive lens surrounding the barrel, consisting of a combination of fast and slow explosives, permitted the launch tube to be imploded with a prescribed phase velocity in excess of the VOD of the explosives used. Using this approach, PI launched an intact 2 g projectile to a velocity of 12.2 km/s,[6] which remains a world-record velocity for projectile masses greater than 1 g.

While the velocities demonstrated by the PI implosion-driven hypervelocity launcher are impressive, the detailed design process and a thorough characterization of the dynamics of the launcher pump tube were not reported. This study was undertaken to examine the dynamics of imploded tubes with systematic parametric investigations to identify the governing physical principles, the ultimate goal being optimization of a device to be used as the pump tube for hypervelocity launchers or a shock tube capable of generating extremely high temperature (>20,000 K) and pressure (>1000 atm) shock waves in gases. The current paper describes an experimental investigation in which the tube dimensions, fill pressure, and explosive loading (tamped and

[a)]Electronic mail: daniel.szirti@mail.mcgill.ca.

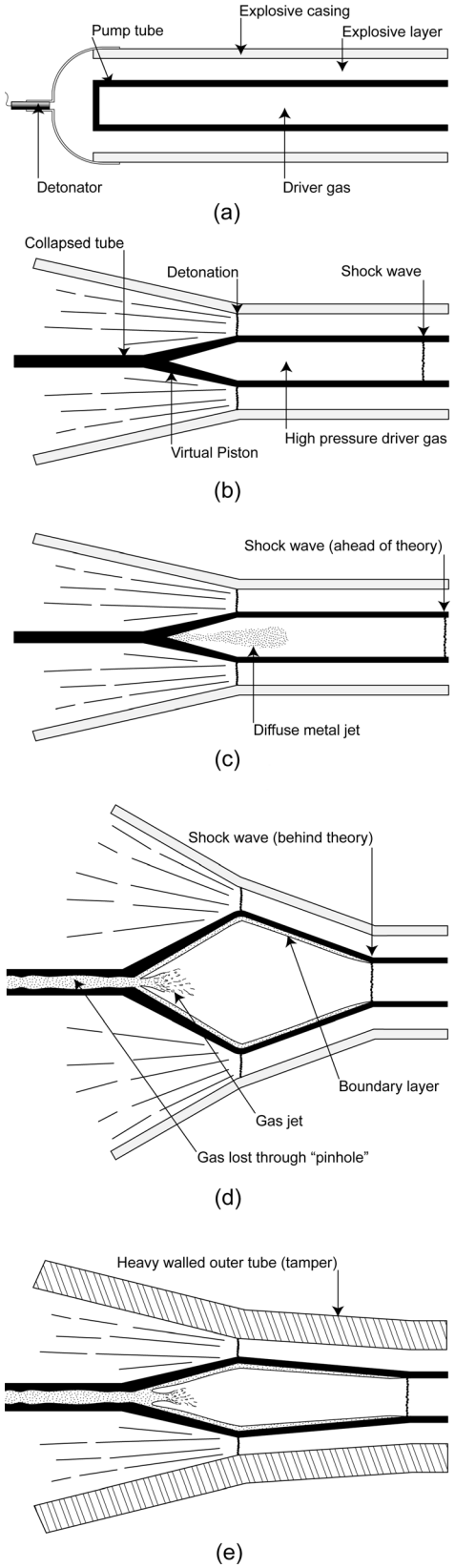

FIG. 1. Explosively driven imploding pump tube showing (a) pump tube before detonation, (b) ideal pump tube operation, (c) initial stages of operation, (d) nonideal operation, and (e) tamped operation.

untamped) were systematically varied in order to identify and, where possible, quantify limiting effects. The paper also presents an analytical model based on acoustic wave interactions that was developed to calculate the effects of pump tube expansion on the PSW velocity and standoff distance.

II. EXPLOSIVELY DRIVEN SHOCK TUBES

A. Ideal theory

Ideally, the implosion pinch is impermeable and acts as a piston traveling down the pump tube at the VOD of the explosive. This results in the formation of a PSW traveling ahead of the piston. For a perfect gas, the Mach number M_s of a shock wave propagating into an initially quiescent gas can be obtained through the following relation:

$$\frac{U_p}{c_0} = \frac{2}{\gamma + 1}\left(\frac{M_s^2 - 1}{M_s}\right),$$

where U_P is the velocity of the piston, c_0 is the initial sound speed in the gas, and γ is the ratio of the specific heats of the gas. For example, if nitromethane is used as the explosive (VOD $\approx$ 6 km/s) and helium as the driver gas ($\gamma = 1.667$), one would expect an 8.1 km/s PSW. Since the PSW travels faster than the piston, as it moves further down the tube the separation between the piston and the shock (called standoff distance) increases and ideally is only limited by the length of the tube. Ideally, the walls of the pump tube are considered rigid and the PSW velocity and the standoff distance are independent of pressure. The ideal standoff distance x_{st} is given by:

$$x_{st} = x_s - x_p,$$

where x_s is the position of the PSW and x_p is the position of the virtual piston. In the experiments presented in this study, the standoff was measured when the PSW reached a defined position down the pump tube, so x_s is known. The position of the virtual piston at this time is given by:

$$x_p = U_p t_s = U_p \frac{x_s}{U_s},$$

where t_s is the time at which the PSW reaches x_s and U_s is the PSW velocity. Then the ideal standoff becomes:

$$x_{st} = x_s - U_p \frac{x_s}{U_s} = x_s\left(1 - \frac{U_p}{U_s}\right).$$

This means that, in the ideal case, the standoff distance measured at a certain position down the pump tube is only dependent on the ratio of PSW velocity to the virtual piston velocity, which, for strong shocks, depends on the type of driver gas used.

The pressure and temperature behind the shock can be easily obtained through normal shock relations:

$$\frac{p_s}{p_0} = \frac{2\gamma M_s^2 - (\gamma - 1)}{\gamma + 1},$$

$$\frac{T_s}{T_0} = \frac{\left[2\gamma M_s^2 - (\gamma - 1)\right]\left[2 + (\gamma - 1)M_s^2\right]}{(\gamma + 1)^2 M_s^2},$$

where the subscripts *0* and *s* denote the initial and shocked states, respectively. The speed of sound behind the shock, c_s, can be obtained through the following relation:

$$c_s = \sqrt{\gamma R T_s},$$

where R is the specific gas constant. For the example given above, the Mach number of the shock is approximately 8.0. This gives a pressure ratio across the shock of 80 and a temperature ratio of 21. For a driver filled with helium at 20 atm and 300 K, this means the pressure, temperature, and speed of sound behind the shock are approximately 1600 atm, 6300 K, and 4.6 km/s.

B. Nonideal effects

Previous work on tube implosion has showed that there are a number of nonideal effects which may affect the behavior of the pump tube. Moore[5] hypothesized that there are three main nonideal phenomena: radial expansion of the pump tube behind the PSW, the development of a boundary layer behind the PSW, and the formation of a diffuse metal jet by the collapsing pump tube. These are depicted in Figs. 1(c) and 1(d).

The shocked driver gas pressure usually exceeds the yield strength of the pump tube, causing the tube to expand radially and generate rarefaction waves which attenuate the PSW. The importance of this effect increases as the PSW gets further ahead of the virtual piston, until the tube expands to the point of rupture. Experiments by Moore[5] showed that as the initial fill pressure of the driver gas increases, the velocity of the PSW decreases and leads to shorter standoff distances. Although this can be prevented by increasing the wall thickness of the pump tube, a more effective method is to surround the explosive layer by a thick-walled tube called a tamper, as shown in Fig. 1(e). The tamper prevents pump tube expansion and focuses the effect of the explosives toward the axis such that a given tube may be collapsed by thinner explosive layers.[3,5]

As with shock tubes, the relative motion of the shocked gas against the pump tube wall causes a boundary layer to develop behind the PSW. The gas inside the boundary layer receives little forward acceleration and leaks past the pinch of the collapsing tube, resulting in a loss of shocked driver gas, which attenuates the PSW until the mass of gas entering the shock equals the mass of gas lost to the collapsing pump tube.[3,5] At this point, a steady state is reached where the shock travels at the VOD of the explosive and the length of shocked gas attains a maximum value. A very similar phenomenon called the "channel effect" was observed in channels lined with high explosive in which there was no metal tube wall between the explosive and the gas.[9–11] Mirels[12] performed an analysis to estimate both the final separation distance between the shock and the contact surface in a shock tube experiment and the variation of this separation distance with respect to the distance traveled by the shock. This analysis, however, neglects the communication time between the piston and the shock front. Waldron *et al.*[3] and Watson[6] found that incorporating this communication time yields much better results when compared to experiments with explosive-wrapped tubes.

Implosively collapsing tubes is a known way of obtaining high-velocity metal jets; Moore[5] obtained photographic evidence of the presence of such a jet when collapsing pump tubes with an initial fill pressure below 15 atm. Unusually high PSW velocities, up to twice the ideal value, were recorded in such experiments and the photographs showed that the jet material was well-mixed with the driver gas; such a jet is depicted in Fig. 1(c). When the collapsing pump tube wall reaches the central axis, a shock wave forms in the tube wall material which turns the material flow behind the pinch along the axis of the tube. This shock has a maximum turning angle beyond which it cannot turn the whole flow into the axial direction, resulting in some of the tube material being jetted ahead of the pinch. If the inner collapse angle (the angle between the collapsing wall of the tube and the axial direction) of the pump tube is less than this maximum turning angle, no jet is formed. Waldron *et al.*[3] performed qualitative numerical simulations to approximate collapse profiles for different conditions and showed that a higher driver gas pressure inside the pump tube and a thicker tube wall would diminish the collapse angle. However, since the mass of the jet is a fraction of the tube mass, using a thinner tube wall would also minimize the mass of the jet. A tamper, by delaying the expansion of the detonation products, maintains a higher pressure on the pump tube for a longer period of time, leading to larger inner collapse angles and a larger mass of jetted material. The maximum turning angle can be made greater by increasing the Mach number of the pump tube wall material flow by using an explosive with a higher VOD and a tube material having a lower sound speed. Note that the jetting and boundary layer effects are closely related: the initial jet is entirely composed of pump tube wall material, but as the boundary layer thickness increases, the jet will become more and more composed of boundary layer gases; ultimately some boundary layer gas may be swallowed by the collapsing pump tube and the entire jet will be composed of the remaining boundary layer,[3,5] as shown in Fig. 1(d).

It is also possible to use the jet as the piston itself, resulting in higher piston velocities. Gill and Goettelman[13] and Gill[14] used glass pump tubes to generate a diffuse glass particle jet initially traveling at twice the VOD in order to drive a PSW. They reported that there was no mixing of glass particles with the shocked gas. However, the initial fill pressure of the gas into which the piston travels needs to be low (on the order of 1 atm). Higher pressures will also cause the glass tube to break after being exposed to PSW pressure.

Besides these three main mechanisms, other nonideal effects were noticed in previous investigations and should be taken into consideration. Typically, extremely high pressures and temperatures are achieved during driver operation, of the order that may influence the driver gas properties by causing ionization or dissociation. Using the Saha equation of state, Watson[6] showed that helium behaves as an ideal gas for very high pressures and temperatures, making helium a good choice of driver gas. Glenn and Crowley[15] reported that heat transfer and friction can be responsible for slowing down the PSW. This effect was observed after 6 m of travel in a 7.8 cm ID tube, or 77 diameters. Results from Matyushkin and Trishin[16] indicate that the inner layers of collapsed shells were vaporized by the conversion of kinetic energy into heat, resulting in an inner channel within the collapsed shell.

TABLE I. Experimental details for all shot series.

Shot series	Pump tube dimensions	Outer tube dimensions	Explosive layer thickness	Position of measurements
0.64 cm OD untamped	0.64 cm OD, 0.46 cm ID	2.22 cm OD, 1.59 cm ID PETG plastic	0.48 cm	52 cm
1.27 cm OD tamped	1.27 cm OD, 1.09 cm ID	4.45 cm OD, 1.91 cm ID steel	0.32 cm	125 cm
1.27 cm OD untamped	1.27 cm OD, 1.09 cm ID	3.18 cm OD, 2.54 cm ID PETG plastic	0.64 cm	125 cm

Schreffler and Christian[17] observed a disturbance along the inner tube wall surface ahead of the shock caused by radiation from the shock front and Savrov and Ageev[18] found that it is possible for the tube walls to be evaporated due to precursor radiation. Further investigation by Jones and Davis[19] showed that the expansion of radiatively heated gas along the tube wall can generate a precompressed gas layer ahead of the shock. Although Schreffler and Christian did not observe this phenomenon when using helium as a driver gas and Jones and Davis did not use helium because it yields little light emission, it is possible that this effect was present in the current study.

III. EXPERIMENTAL DETAILS

Experiments were performed to ascertain the dynamics of the precursor shock as a function of the initial fill pressure of the pump tube. Different sizes of pump tubes were investigated and the effect of adding a tamper was examined.

A. Charge design

Experiments were carried out using two different pump tube sizes: 0.64 cm outer diameter (OD) by 0.46 cm inner diameter (ID) and 1.27 cm OD by 1.09 cm ID. The tubes were made of 304 stainless steel. The 0.64 cm OD tubes were surrounded by a 4.8 mm thickness of explosive which was contained in a thin-walled outer tube made of glycol-modified polyethylene terephthalate (PETG). Two different configurations were used with the 1.27 cm OD tube in order to examine the effect of a tamper: a 3.2 mm thickness of explosives with a 1.27 cm thick steel outer tube and a 6.4 mm thickness of explosives with a thin PETG outer tube. The details of each series are given in Table I; a schematic of the apparatus is shown in Fig. 2(a) and typical cross sections of tamped and untamped pump tubes are shown in Fig. 2(b). The explosive used was nitromethane sensitized with 10% diethylenetriamine (DETA), a liquid explosive having a VOD of 6 km/s and a detonation pressure of 11 GPa.[20] The failure thickness for this explosive confined in polyvinylchloride is 2 mm.[21] When confined in steel, the failure thickness is further reduced;[22] therefore detonation failure due to an insufficient thickness is not a concern. The downstream end of the pump tube was capped; the tube was pressurized with helium via a fill line connected to the upstream end to initial pressures from 10 atm to 100 atm.

B. Diagnostics

The outer tube was instrumented with self-shorting twisted wire pair (SSTWP) gauges. These gauges consist of two wires forming an open circuit which are twisted together and inserted directly into the explosive; as soon as the detonation reaches them, the detonation pressure causes the wires to short, discharging a capacitive circuit. An oscilloscope records the time of arrival of the detonation at the gauge location. It is assumed that the axial location of the virtual piston (the pinch or implosion point) was coincident with the detonation front. The pump tube was instrumented with piezoelectric sensors (shock pins, Dynasen CA-1135). These are uncalibrated sensors which convert any applied pressure into a signal which is recorded by an oscilloscope. The

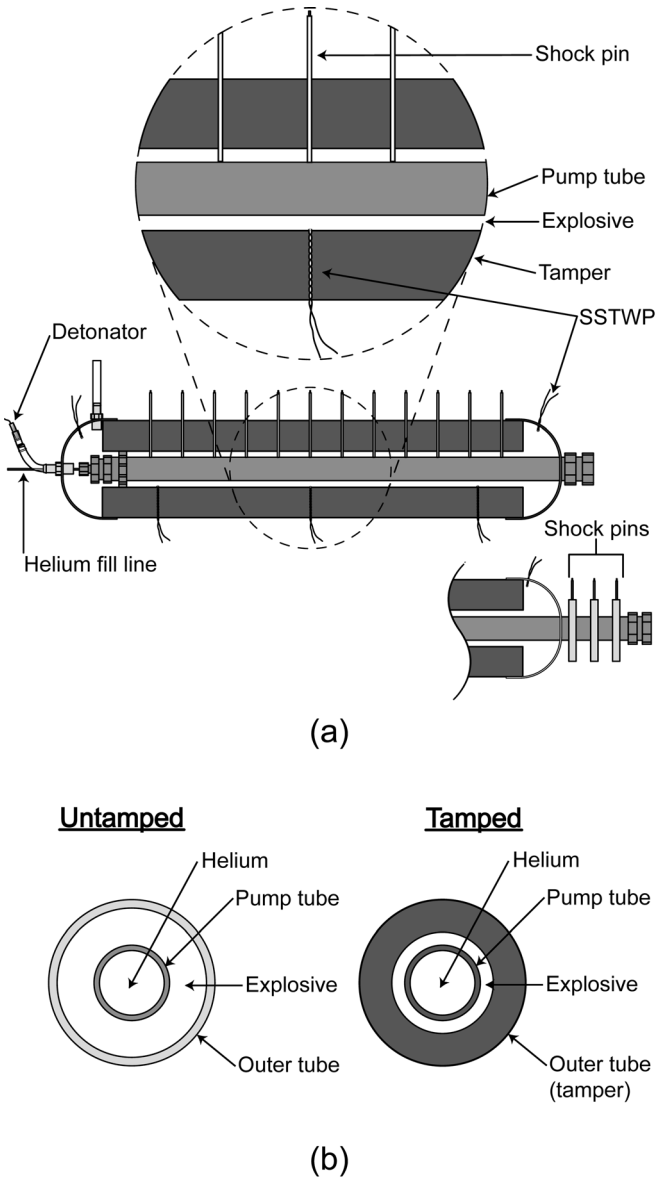

FIG. 2. Experimental set-up for investigation of the precursor shock wave in an imploding tube. (a) Driver experimental setup with instrumentation and (b) typical driver cross-sections.

arrival of the PSW is indicated by a large and rapid rise in the signal; slopes of 400 V/μs are typical. In some cases, the entire length of the pump tube was instrumented with shock pins and SSTWP gauges, while others only had SSTWPs at the extremities of the outer tube and shock pins on a section of the pump tube extending beyond the explosive [see Fig. 2(a)]. Data obtained from both versions was compared and found to be identical within experimental error.

Detonation and precursor shock velocities as well as standoff distance were determined from the position-time data obtained from the SSTWPs and the shock pins. The detonation and shock velocities were taken as the slope of a linear fit to the SSTWP and shock pin signals, respectively, in the region of interest. The standoff distance and shock velocity were obtained after the shock had traveled 115 internal pump tube diameters beyond the initial collapse point, which is the point where the detonation entered the outer tube.

IV. RESULTS

A. Visual examination

For the 0.64 cm OD series, recovered collapsed pump tubes were sectioned approximately 15 cm from the initial collapse point to verify whether they had been completely collapsed or not. Figure 3(a) shows that a small hole remained at the center of the tube. This hole was larger for higher initial fill pressures. The recovered tubes for trials under 25 atm initial fill pressure were relatively straight and intact. However, as the initial fill pressure was raised beyond that point, recovered tubes showed signs of axial rupture, as shown in Fig. 3(b), particularly further downstream. Because of this, the entire length of the pump tube could not be recovered, shorter lengths being recovered for higher fill pressures, as shown in Fig. 3(c). This was also the case for 1.27 cm OD tubes, both tamped and untamped, although the recovered pump tube sections for the tamped series were always longer than the corresponding untamped tubes. This suggests that tamped pump tubes are better able to contain the high-pressure driver gas, resulting in a greater length of shocked gas.

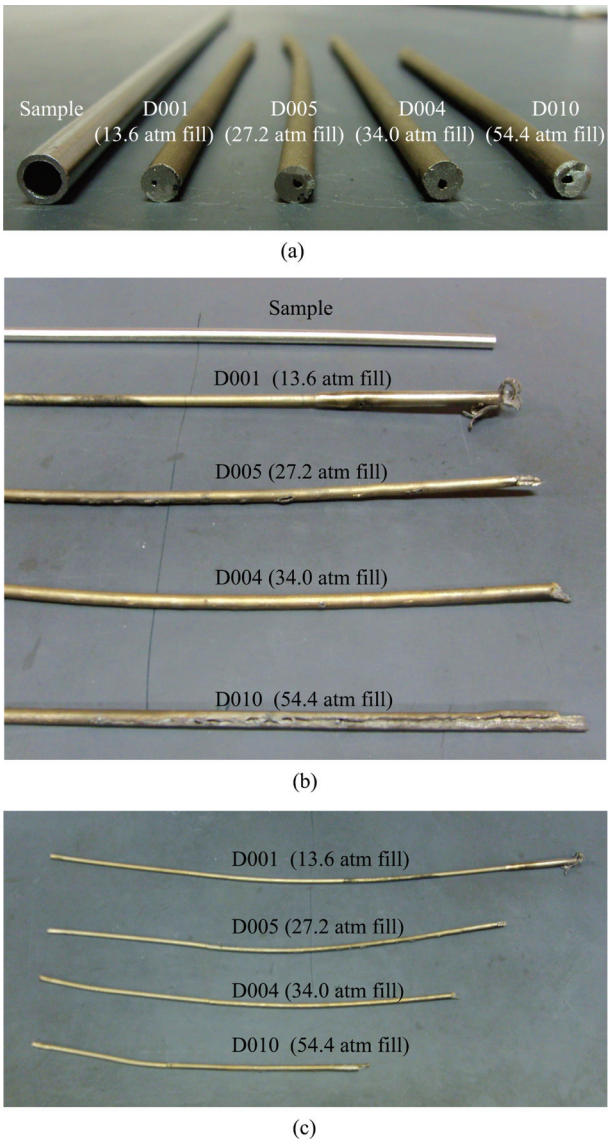

FIG. 3. (Color online) Photographs of recovered 0.64 cm OD pump tubes. (a) Pump tube cross sections taken 15 cm from the initial collapse point, (b) recovered pump tubes showing rupturing along the length, and (c) recovered length of the pump tube tends to decrease with increasing initial fill pressure.

B. Shock velocity and standoff measurement

Figure 4 shows the data obtained for a typical experiment in the 1.27 cm OD tamped series. The fill pressure for this tube was 20.4 atm, and the length of the tube was 1.5 m. The SSTPW gauges measured a VOD of approximately 6.6 km/s, which is faster than the expected VOD of nitromethane; this effect will be discussed in Sec. IV.C. A piston traveling at that speed would generate an 8.9 km/s shock in helium. Shown in Fig. 4(a) are the measured shock and detonation waves, as well as the ideal shock trajectories for 6.0 km/s and 6.6 km/s pistons. The measured shock trajectory falls between the two curves.

The shock pin data indicates that the PSW was initially traveling at a speed of approximately 10 km/s, which is faster than the 8.1 km/s predicted by theory; at the end of the tube, the velocity had decayed to approximately 7 km/s [see Fig. 4(b)] and does not appear to have reached a steady value. The standoff distance was approximately 30 cm by the end of the pump tube [see Fig. 4(c)].

The PSW required some time to emerge ahead of the detonation front. Although the PSW velocity decayed as it traveled further down the pump tube, by taking the PSW velocity recorded from the two first shock pin signals and extrapolating the trajectory back to where it intersects the detonation trajectory, a conservative estimate on the distance traveled by the PSW before it emerged ahead of the detonation front can be obtained. This distance was 12.2 cm for this experiment, or approximately 10 inner pump tube diameters. A distance of 10 diameters was typical of most experiments in each shot series.

The calculated curves in Figs. 4(b) and 4(c) are obtained from the analytical model presented in Sec. V. This model calculates the standoff and PSW velocity while taking pump tube expansion into account. Model calculations are also given where the PSW velocity is initialized at twice the

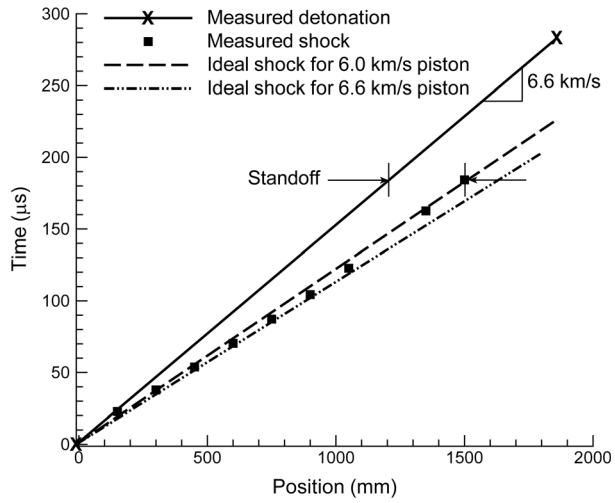

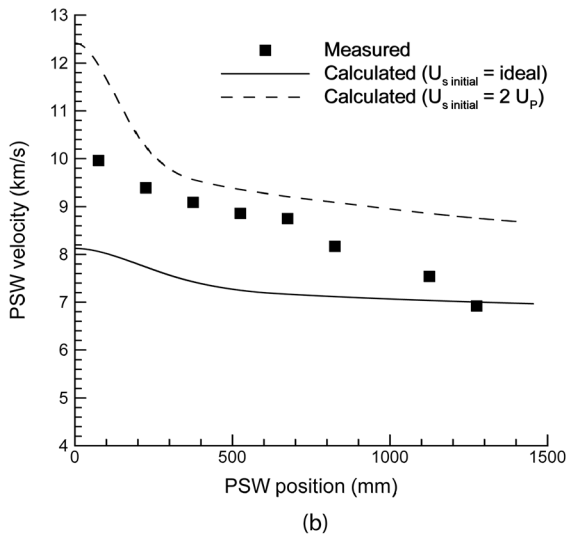

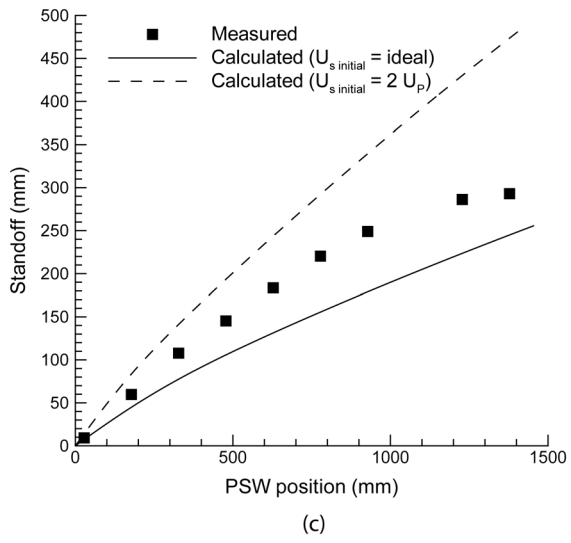

FIG. 4. Typical results for a 1.27 cm OD tamped pump tube with 20 atm initial fill pressure. (a) Detonation and PSW trajectories, (b) PSW velocity versus PSW position, and (c) standoff versus PSW position.

virtual piston velocity ($U_{s\ initial} = 2U_P$) to account for the initial presence of jetting. In practice it takes approximately 10 diameters for the shock to form, but the model assumes that the shock forms immediately; thus, the experimental shock data was spatially offset to the origin for Figs. 4(b) and 4(c). In model calculations the standoff distance and PSW velocity are therefore measured after 105 internal pump tube diameters of travel instead of 115.

Figure 5 shows the standoff and shock velocity data measured at 115 diameters of PSW travel versus initial fill pressure for the 0.64 cm untamped pump tube series. The standoff and PSW velocity decrease with fill pressure. This is primarily due to the radial expansion of the pump tube caused by the high shocked pressure of the driver gas between the PSW and the virtual piston. At low (10–15 atm) initial fill pressures, the standoff is higher than the ideal

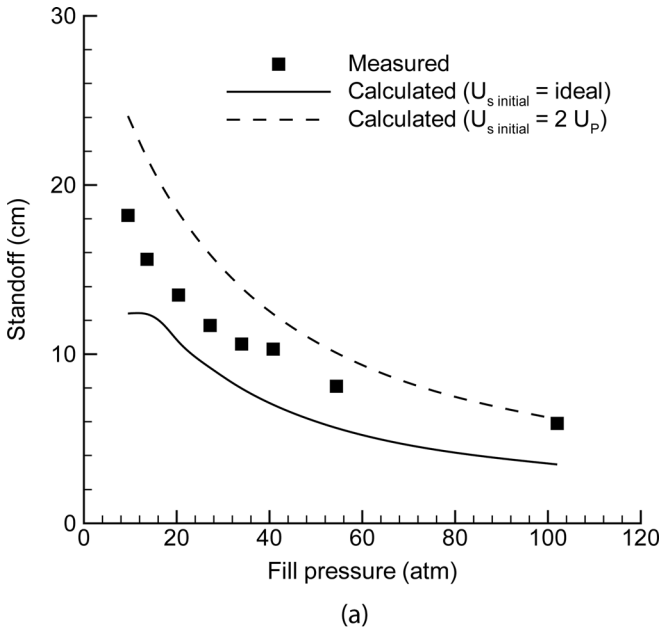

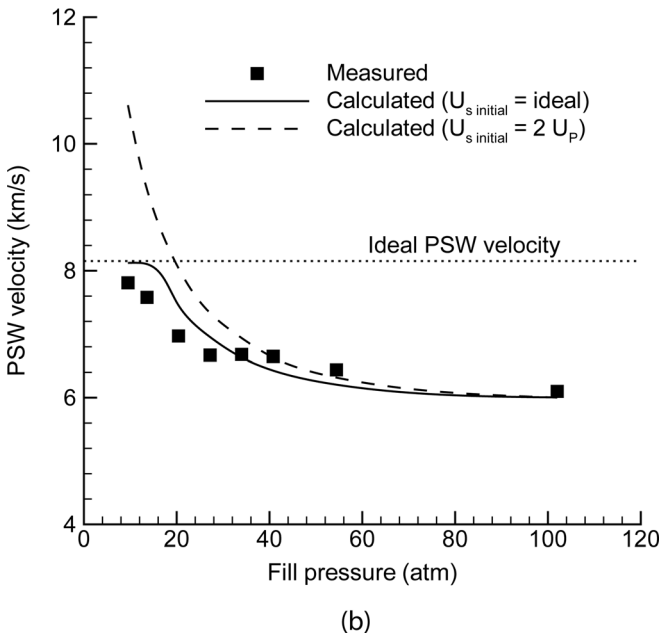

FIG. 5. Summary of results with a 0.64 cm OD pump tube and corresponding model results, showing (a) the PSW standoff from the detonation front and (b) the PSW velocity, both measured 115 diameters after the initial collapse point.

value, yet the shock velocity is less than the ideal value. This is attributed to jetting of tube material and a possible radiation precursor. This effect is not seen at higher pressures (above 20 atm).

The results from the 1.27 cm pump tube series, both tamped and untamped, are shown in Fig. 6. Figures 6(a) and 6(b) show the standoff and PSW velocity data, respectively, for the tamped case, and Figs. 6(c) and 6(d) show the data for the untamped case. The 1.27 cm untamped standoff falls below that of the 1.27 cm tamped series, suggesting that pump tube expansion has a substantial impact on standoff and that adding a tamper is an effective way to limit this expansion.

For the 1.27 cm tamped series, the PSW velocity initially decreases with fill pressure but increases for pressures exceeding 50 atm [see Fig. 6(b)]; standoff distance also increases slightly at the highest pressure. This may be due to precompression of the nitromethane, leading to an increased VOD which would drive a faster PSW, as explained in the next section. This may also be due to rupturing of the pump tube caused by the high shocked driver gas pressure. The resulting loss of driver gas would relieve the pressure inside the pump tube, allowing the virtual piston to re-form further on, restarting the whole process. This would result in cyclical breaking up and reforming of the virtual piston and thus oscillations in the PSW. On reforming, the resulting restarted PSW is expected to travel faster than the ideal velocity due to initial jetting. The recorded PSW data in the region of interest would then be a snapshot of this transient process. The data obtained for a 1.27 cm OD tamped pump tube with an initial fill pressure of 70 atm showed the PSW velocity oscillating between 7 and 9 km/s, which supports the rupturing theory above. The SSTWPs are believed to have been triggered by the PSW in this experiment, recording velocities oscillating between 7 and 8.4 km/s very near the shock pin signals; therefore, no reliable VOD or standoff distance measurement could be made.

There is no discernable pattern for shock velocity for the 1.27 cm OD untamped series [see Fig. 6(d)]. This may be caused by pump tube bursting, resulting in a transient regime as explained above; for untamped pump tubes, it is very unlikely the pressure in the nitromethane ever reaches a point where it could significantly influence the detonation.

Results of model calculations are also shown on Figs. 5 and 6; these are discussed in Sec. V.B.2.

C. High velocity of detonation due to precompression

For the tamped 1.27 cm OD series, the VOD increased with increasing initial fill pressure and the cause was assumed to be the precompression of the nitromethane as it gets squeezed between the tamper and the expanding pump tube. Since the VOD increases with explosive density, the compression of the explosives under the action of the expanding tube results in an increase of the VOD. A similar phenomenon was also observed to occur with the channel effect.[10]

Experiments were performed to rule out the possibility that the PSW was prematurely shorting the SSTWP gauges by positioning the SSTWPs in regions of the explosive that

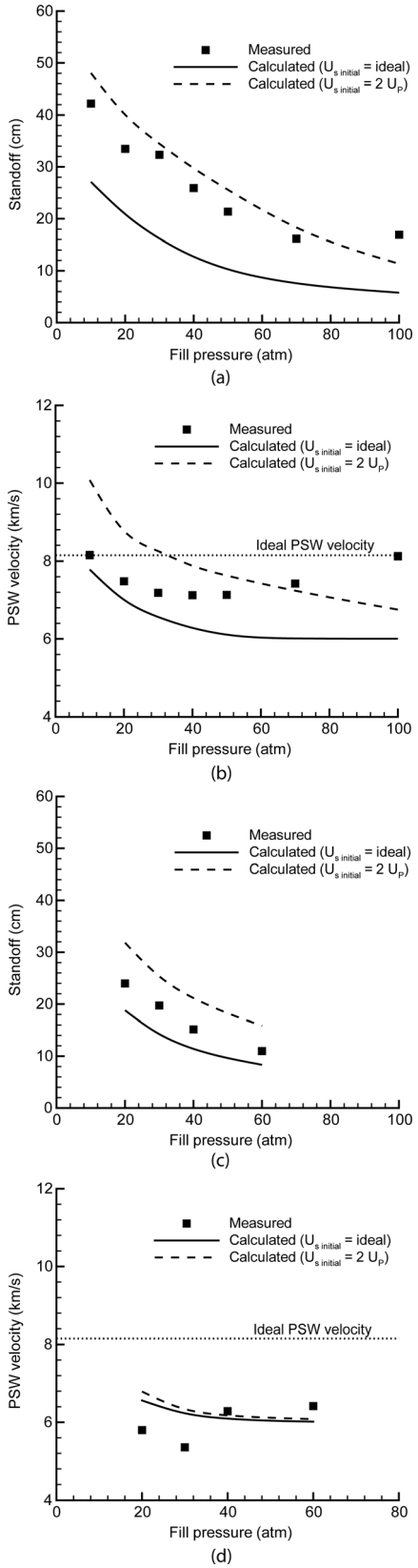

FIG. 6. Summary of results with a 1.27 cm OD pump tube and corresponding model results, showing (a) the PSW standoff for the tamped series, (b) the PSW velocity for the tamped series, (c) the PSW standoff for the untamped series, and (d) the PSW velocity for the untamped series, all measured 115 diameters after the initial collapse point.

were unaffected by the PSW. Results from these experiments demonstrate that the SSTWP gauges were indeed recording the detonation wave and that the increase in VOD is a real phenomenon.

Assuming the tamper did not yield from internal pressures, a static analysis on the system shows that the pressure in the explosive was equal to the shocked driver gas pressure. This assumption has been verified with the analytical model presented in Sec. V; results from the model indicate that the explosive layer pressure eventually oscillates near the driver gas pressure. It is then possible to calculate the density of the compressed nitromethane using the Winey-Gupta equation of state for nitromethane.[23] Subsequently, the VOD can be calculated using Cheetah.[20] In Fig. 7, the recorded VODs for the 1.27 cm tamped series are plotted against the results obtained from Cheetah using the newc1 product library, which is a renormalized Becker-Kistiakowsky-Wilson (BKW) library with a three-phase carbon equation of state. The results from Cheetah fall beneath the measured data. This indicates that the pressure reached by the nitromethane may be underestimated in calculations, but it seems clear that the increased velocity of detonation recorded is due to a precompression of the nitromethane caused by the swelling of the pump tube.

A slight rise in VOD was also observed in the 1.27 cm untamped series; however, without a tamper, the compression of the nitromethane layer is limited and as a result the VOD is not increased significantly.

The consequences of this effect are to increase the PSW velocity and thus the shocked driver gas pressure, which leads to a faster rate of expansion of the pump tube and a slightly lower standoff. However, the change in PSW velocity and VOD themselves should have no effect on the standoff since the ratio between these values remains the same.

V. ANALYTICAL MODEL OF NONIDEAL OPERATION

Experimental results and previous work[6] suggest that expansion and rupture of the pump tube may be the main nonideal phenomenon affecting the performance of the pump tube. It is therefore important to understand the dynamics of pump tube expansion through a simple analytical model. In so doing, it will be possible to gauge the effects of the various parameters influencing the system. These include the initial driver gas fill pressure, the pump tube radius and wall thickness, the thickness of the explosive layer, and the material properties of the tube and the explosive. The model should also quantify the effect of adding a tamper surrounding the explosive. Because of the dynamic nature of pump tube operation, the tube may not reach a static equilibrium state. The tube may be expanding until it is collapsed by the detonation wave. The role of the tamper in this regard is a dynamic one: an adequate pressure has to buildup in the intervening explosive layer before the tamper can noticeably confine the pump tube. The static equations are therefore not enough to model these effects and a dynamic model is needed.

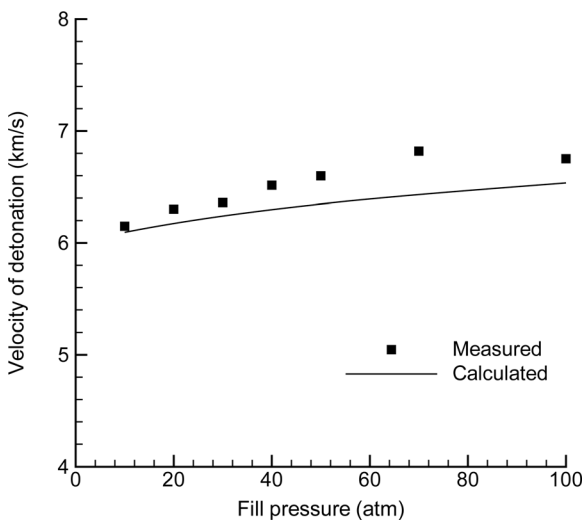

FIG. 7. Experimental measurement of the VOD of liquid nitromethane in tamped pump tube experiments.

A. Tube expansion dynamics

1. Pump tube motion

Consider a cross section of the pump tube, located some distance x_0 down the tube. The tube will be subjected to an instantaneous change in internal pressure once the shock wave passes x_0. The problem is axisymmetric, which means that the tube will expand uniformly and remain circular. It will also be assumed that the inclination of the tube wall with respect to the central axis is negligible. This is analogous to a cylindrical piston which is driven outward via a constant internal pressure. Newton's second law can be applied to a one-dimensional segment of the cross section. See Fig. 8 for a sketch of the tube segment and forces acting on it.

Consider an elementary segment, such that the angle $d\theta$ is small. The pump tube has radius r and thickness τ. Pump tubes are typically thin-walled tubes, which means that only hoop stress (σ_h) needs to be considered (hoop stress can also be assumed to be constant throughout the thickness). The tube experiences both internal pressure, $p_{internal}$, from the shocked driver gas contained within, and external pressure, $p_{external}$, from the liquid explosive surrounding it which is being compressed by the expanding tube. As will be shown later, $p_{external}$ depends on the radius and wall speed of both

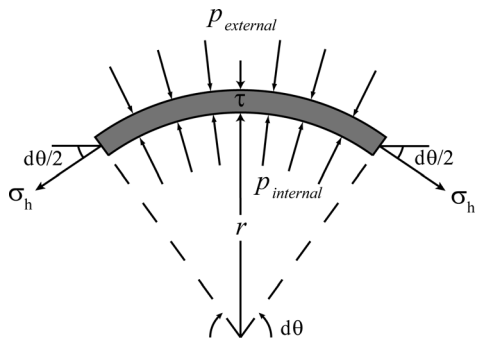

FIG. 8. Force balance on a pump tube segment.

the pump tube and the outer tube. Applying Newton's second law in the radial direction and using the small angle approximation one obtains the following differential equation:

$$\ddot{r} = \frac{\left[p_{internal} - p_{external}\left(r_{pt}, \dot{r}_{pt}, r_{ot}, \dot{r}_{ot}\right)\right]}{\tau \rho_{tube}} - \frac{\sigma_h}{r \rho_{tube}}, \quad (1)$$

where ρ_{tube} is the density of the tube material and the subscripts *pt* and *ot* stand for "pump tube" and "outer tube," respectively. From conservation of mass, assuming the tube material is incompressible, the tube thickness decreases as it expands according to the following equation:

$$\tau = \frac{r_0 \tau_0}{r}, \quad (2)$$

where r_0 is the initial pump tube outer radius and τ_0 the initial pump tube thickness. Combining Eqs. (1) and (2), gives:

$$\ddot{r}_{pt} = \left\{ \frac{\left[p_{internal} - p_{external}\left(r_{pt}, \dot{r}_{pt}, r_{ot}, \dot{r}_{ot}\right)\right] r}{r_0 \tau_0 \rho} - \frac{\sigma_h}{r \rho} \right\}_{pt}. \quad (3)$$

Typically, the pump tube experiences very high strain rates during expansion since it is being instantaneously loaded with a very high internal pressure. Calculated maximum strain rates for the pump tube vary between the order of 10^3 s^{-1} and 10^4 s^{-1}, depending on fill pressure. Static values for stress and strain do not apply, therefore a model dependent upon strain rate (a function of both r and $\dot{r}$) is needed. Johnson and Cook[24] developed a constitutive model for metals subjected to large strains, high strain rates and high temperatures. This model is widely used in similar problems, such as high-velocity impacts, collapsing liners in shaped charges and explosively formed penetrator devices. Although the range of strain rates over which the Johnson-Cook (JC) model is valid is not explicitly discussed, it uses test data obtained from, among others, torsion tests done over a range of strains rates from quasistatic up to 400 s^{-1}.

The Johnson-Cook strength model defines the von Mises stress σ as the following:

$$\sigma = [A + B\varepsilon^{\eta}][1 + C \ln \dot{\varepsilon}^*][1 - T^{*m}],$$

where ε is the plastic strain, A is the yield stress, B and η are constants which account for strain hardening, the terms in the second bracket account for the effect of strain rate, and the terms in the last bracket account for the effect of temperature. $\dot{\varepsilon}^*$ is the dimensionless plastic strain rate and is given by:

$$\dot{\varepsilon}^* = \dot{\varepsilon}/\dot{\varepsilon}_0,$$

where

$$\dot{\varepsilon}_0 = 1.0 s^{-1}.$$

T* is the homologous temperature and is given by:

$$T^* = \frac{T - T_{room}}{T_{melt} - T_{room}},$$

where T_{room} is the initial temperature of the material and T_{melt} is the melting temperature of the material. All constants — (A, B, η, C, and m) — are determined from tension and torsion tests at different strain rates and temperatures. Note that these values are not readily available for any material, but the accepted values for several materials are given with the JC model.[24] The pump tubes used in experiments reported in this paper were made of 304 stainless steel, but since values for this material are not available, values for 1006 steel were used.

The JC model considers plastic values of stress only. It assumes that the elastic region is negligible, which is valid for high strain rates and large plastic deformations. The linear section of the stress-strain curve is then suppressed and the value of stress at zero strain is the yield stress of the material. The engineering strain is defined as the stretch of the material over its initial length:

$$\varepsilon = \frac{\ell - \ell_0}{\ell_0}.$$

For a tube, the length of the material is equal to the circumference of the tube: $\ell = 2\pi r$. The expression for strain then becomes:

$$\varepsilon = \frac{2\pi r - 2\pi r_0}{2\pi r_0} = \frac{r - r_0}{r_0} = \frac{r}{r_0} - 1.$$

Although the tube is initially at room temperature, it will heat up due to plastic work of deformation; the temperature change can be expressed as:

$$\Delta T = \frac{\beta}{\rho C_p} W,$$

where β is the work rate to heat rate conversion factor and is empirically determined to be approximately equal to 0.9 for most cases, ρ is the density of the material, C_p is the heat capacity of the material, and W is the plastic work of deformation. One can obtain W by integrating the stress-strain curve:

$$W = \int_0^{\varepsilon_f} \sigma d\varepsilon,$$

where ε_f is the final strain reached. In the plastic regime, the stress in the tube will always oppose the motion and any deformation of the tube, even compression following expansion, will generate heat; ε_f is therefore path dependent.

2. Explosive layer pressure

The pressure in the explosive layer is not constant and will fluctuate depending on the movement of its boundaries. When the pump tube expands into the explosive, it will send pressure waves through it. These pressure waves are fairly weak since the fluid speed is small compared to its sound speed. In the case of a liquid explosive, the change in density and sound speed of the explosive will be small enough for the pressure in the explosive layer to be modeled using acoustic waves. Solving for pressure then consists of keeping

track of all the pressure waves transmitted back and forth in the explosive layer. The use of acoustics simplifies the problem since they propagate at the speed of sound in the material, which is assumed constant. Therefore, they are represented as straight lines in a position versus time diagram. This makes it computationally easier to keep track of them, as compared to the more general method of characteristics. Because the acoustic equations are linear, the solution is simply the superposition of the effect of each individual wave.

Even though the geometry is cylindrical, the radius of curvature of the waves generated into the explosive by the expanding piston (the pump tube) is very large compared to the thickness of the wave; the waves can therefore be considered planar. Since the fluid next to the piston has to be traveling at the same velocity as the piston, a change in piston velocity Δu generates an acoustic wave in the fluid, propagating at c_0 (the acoustic speed of the fluid), that changes its velocity by the same amount. The pressure change across this wave is given by conservation of mass and momentum:

$$\Delta p = \rho_0 c_0 \Delta u.$$

If the explosive layer is infinitely thick, these waves propagate outward forever, and the pressure on the tube surface will simply be the sum of each Δp across all the acoustic waves generated up to that point.

If the explosive layer cannot be considered infinitely thick (as is usually the case), the generated acoustic waves will reflect off the outer boundary of the explosive layer. After reflection off the outer boundary, the acoustic waves propagate back and reflect off the pump tube, and thus reverberate back and forth between both boundaries, as shown in Fig. 9(a). For clarity, only one acoustic wave is shown in the figure; in the model, new acoustic waves are generated at each time step, resulting in a net of waves similar to that obtained in the method of characteristics.

Every time a wave goes through a fluid element, the pressure of that fluid element increases by a Δp associated with that wave. Referring to Fig. 9(a) and considering the effect of that single wave, region 1 is at a pressure $p_0 + \Delta p$, region 2 is at a pressure $p_0 + 2\Delta p$, and region 3 is at a pressure $p_0 + 3\Delta p$. The pump tube never actually experiences region 2; it goes directly from region 1 to region 3. Likewise, the outer boundary is never exposed to region 1. Therefore, when a wave reflects off a boundary, the pressure acting on it increases by an amount equal to twice the Δp associated with that wave, so for the pump tube: $p_3 = p_1 + 2\Delta p$, $p_5 = p_3 + 2\Delta p$, and so on.

The case described above is for a single acoustic wave. More generally, there will be a continuum of acoustic waves sent out along the entire surface of the pump tube. For this simplified model, the problem is discretized in time and an acoustic wave is generated every time-step (the time-step size is on the order of 1 to 10 ns). Displaying all the acoustics present in Fig. 9(a) would result in an overly cluttered graph. Instead, zooming-in Fig. 9(a) gives Fig. 9(b), where the acoustic waves sent out at arbitrary times t and t-Δt are shown as well as some acoustic waves generated at earlier

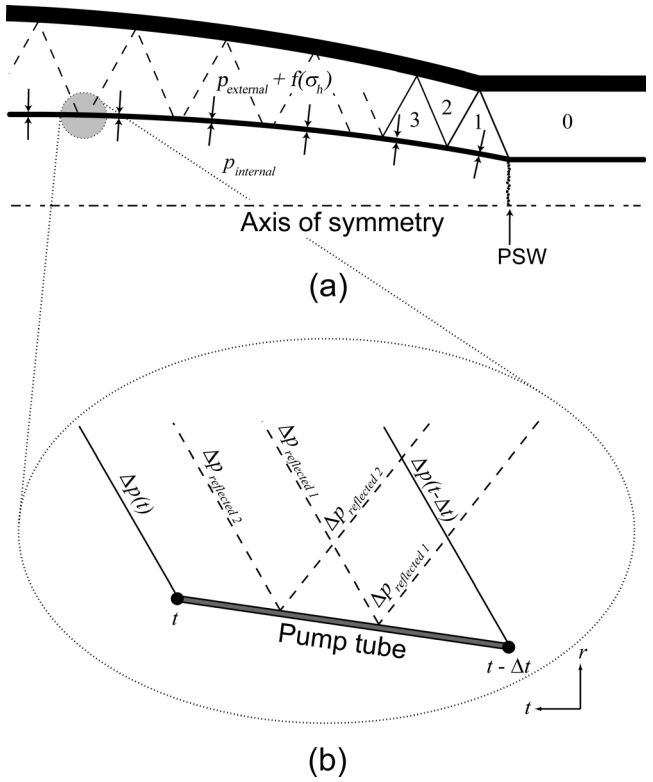

FIG. 9. (a) Position-time graph showing the expanding pump tube and acoustic reverberations. (b) Zoom of the position-time graph of the expanding tube showing one time-step.

times that reflect off the pump tube during that time interval; only two reflected waves are represented in Fig. 9(b), but in practice there may be any number of them. At time t-Δt, the pressure is $p(t\text{-}\Delta t)$, the tube radius is $r(t\text{-}\Delta t)$ and the wall speed is $\dot{r}(t\text{-}\Delta t)$. Based on the difference in internal and external pressures at time t-Δt, the new radius and wall speed at time t, $r(t)$ and $\dot{r}(t)$, can be calculated by solving Eq. (3). The change in wall speed will generate an acoustic wave at time t with a Δp given by:

$$\Delta p(t) = \rho_0 c_0 \Delta u(t) = \rho_0 c_0 [\dot{r}(t) - \dot{r}(t - \Delta t)].$$

Considering the pressure increase due to the reflected waves, the pressure at time t is given by:

$$\begin{aligned} p(t) &= p(t - \Delta t) + \Delta p(t) + 2\left(\Delta p_{reflected_1} + \Delta p_{reflected_2} + \ldots\right) \\ &= p(t - \Delta t) + \Delta p(t) + 2\sum \Delta p_{reflected}, \end{aligned}$$

where the term $\sum \Delta p_{reflected}$ is the cumulative pressure contribution from all the waves which were reflected off the tube during the time-step Δt.

Since the effects of the acoustic waves add up linearly, it is not necessary to keep track of every individual wave generated since the beginning of the calculation. Once these waves interact with a boundary, their effect can be superimposed on the next wave sent out from that boundary; it is therefore assumed that the reflected waves in the above example all interact with the pump tube at time t. The acoustic sent out from the pump tube at time t will include the effects of all the reflected waves as well as the change in

wall speed. This method reduces the number of waves that must be tracked and simplifies the calculation. The error incorporated by using this technique is negligible due to the very small step size and the approximate and discrete nature of the model. The wave sent out from the tube at time t has a total Δp given by:

$$[\Delta p(t)]_{tot} = \Delta p(t) + \Delta p_{reflected_1} + \Delta p_{reflected_2} + \ldots = \Delta p(t) + \sum \Delta p_{reflected}.$$

The $\Delta p_{reflected}$ terms were generated at an earlier point in time, so the pressure at a certain point in time is a function of the pressure at an earlier point in time. The differential equations then become what are known as delay differential equations (DDE). The delay caused by an acoustic wave having to travel back and forth between both tubes is called the *communication time* (t_c) and is equal to the time it takes for an acoustic wave to travel between both tubes. This time is not constant and is a function of the radii of the pump tube and the outer tube, which are functions of time. A wave reaching the outer tube at some time t was generated at the pump tube at some time t-t_c earlier; the radius of the pump tube at time t-t_c must therefore be known. In this case, t_c is given by:

$$t_c = \frac{r_{ot}(t) - r_{pt}(t - t_c)}{c}.$$

A wave reaching the pump tube at some time t was generated at the outer tube at some time t-t_c earlier, so when considering a wave traveling from the outer tube to the pump tube, t_c is given by:

$$t_c = \frac{r_{ot}(t - t_c) - r_{pt}(t)}{c}.$$

The pressure in the explosive layer therefore depends on both r and $\dot{r}$ of the pump tube and the outer tube. The functions for t_c are implicit. In the numerical solver, it is necessary to iterate to find t_c for each wave traveling between the pump tube and the outer tube.

3. Outer tube motion

The motion of the outer tube surface in reaction to the pressure acting on it will generate rarefaction waves. Once these waves reach the pump tube, they will lower the pressure on its surface and allow it to expand faster. In order to help prevent pump tube expansion, it is best to limit the expansion of the outer tube, ideally with a rigid outer tube, as in Fig. 9(a). A heavy-walled tube made of a strong and dense material, such as steel, will better contain the pressure within it, thus reducing and delaying pump tube expansion. The effect of the tamper will be felt by the pump tube more quickly if the communication time is small, which means a thin layer of explosive is best when using a tamper. The differential equation governing the outer tube motion is very similar to that governing the pump tube motion, except it will only be subjected to the internal pressure from the liquid explosive it contains:

$$\ddot{r}_{ot} = \left[\frac{p_{internal}(r_{pt}, \dot{r}_{pt}, r_{ot}, \dot{r}_{ot})r}{r_0 \tau_0 \rho} - \frac{\sigma_h(r)}{r\rho}\right]_{ot}.$$

Analytical expressions for the behavior of a thick-walled tube which is subjected to high strain rates and large plastic deformations are not available; typically, finite element methods are used in these cases. For simplicity, the thin shell approximation was used to find the hoop stress. Since pressures experienced by the tamper and the pump tube will eventually oscillate near the driver gas pressure, it is recommended to make the tamper thick enough to contain pressures slightly above the PSW pressure. In the untamped case a thin plastic tube is typically used to contain the explosive and its strength can be neglected ($\sigma_h = 0$).

4. Calculated expansion histories

The differential equations governing the pump tube and outer tube motions were integrated using a fourth-order Runge-Kutta method. The stresses and pressures were obtained using a forward difference method within the main loop of the calculation. In all cases, convergence was verified by altering the time-step size until the results were found to converge; time-steps in the range of 1 to 10 ns were typical.

The model outputs the pump tube radius and the outer tube inner radius as a function of time. Various parameters can easily be varied, such as pump tube diameter or initial fill pressure, to investigate their effects on the expansion of the pump tube.

A design requirement is that the pump tube does not burst before the detonation can reach and implode it. Since the shock is traveling faster than the detonation, the longer the pump tube is, the farther ahead of the detonation the shock will get, and the longer it will have to contain the pressure without bursting. However, it is difficult to predict when the pump tube will burst under conditions of high strain rate and large plastic deformations. For this study, it was considered that the tube failed once it reached 30% elongation, the same criterion used by Watson.[6]

Figure 10 shows expansion histories for a 1 m long, 1.27 cm OD, 1.09 cm ID tube. The explosive layer thickness is 3.2 mm. Assuming ideal PSW conditions, the tube has to hold pressure without bursting for approximately 45 μs; this is the time it takes for the detonation to reach the end of the pump tube after the PSW has passed. Figure 10(a) shows the results for an untamped driver, and Fig. 10(b) shows results for a driver with a 1.91 cm ID, 4.45 cm OD tamper. The bursting pressure for such a tamper is approximately 45 atm. For the untamped case, the pump tube reaches 30% elongation before 45 μs for all pressures shown here. However, for the tamped case, the tamper is capable of dynamically containing the pump tube, which does not reach 30% elongation until beyond 45 μs for all cases. This clearly shows that a tamper can make a substantial difference in preventing or delaying pump tube bursting.

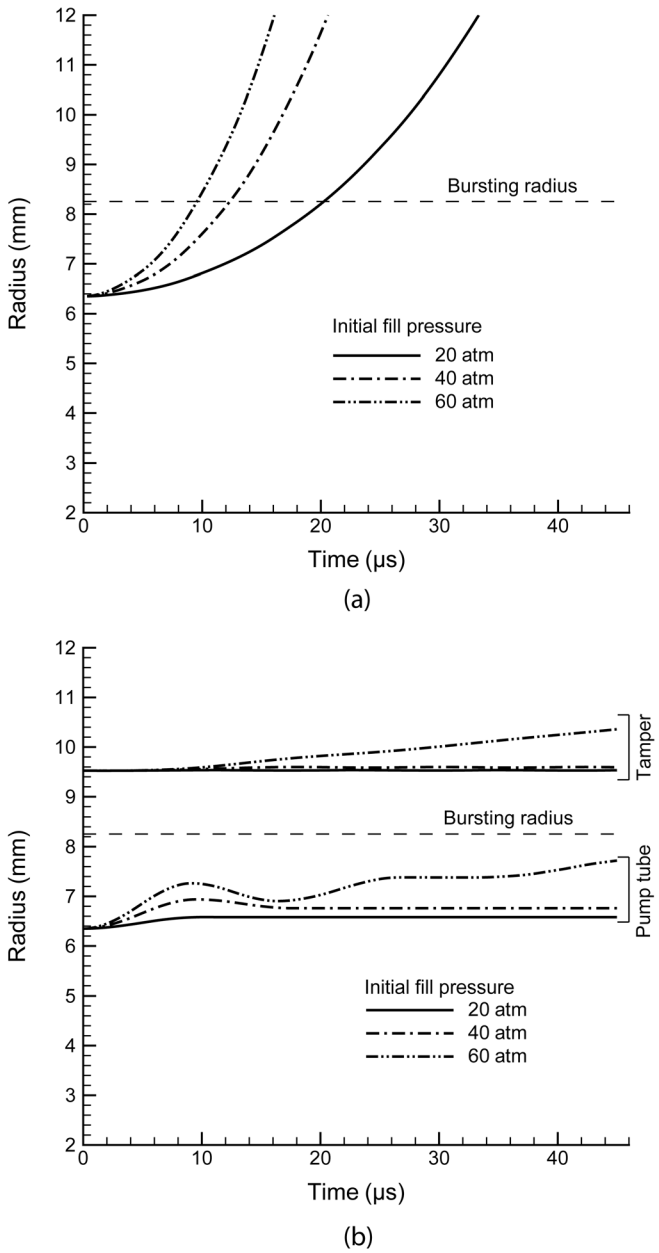

FIG. 10. Expansion histories for (a) untamped and (b) tamped pump tubes.

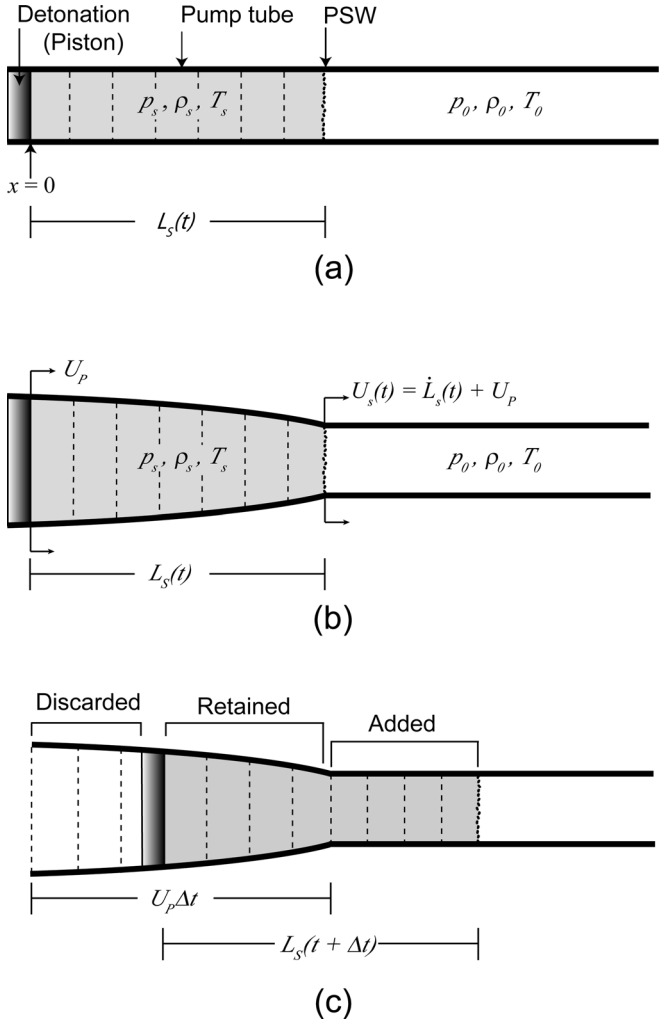

FIG. 11. (a) Dividing the length of tube exposed to PSW pressure into discrete slices, (b) exposed slices expand due to internal pressure, and (c) advancing Δt and re-dividing the length of tube exposed to PSW pressure into slices.

B. Shock Dynamics

1. Shock velocity and standoff distance

In order to validate the model predictions against experimental data, the model developed above needs to predict PSW velocity and the standoff distance based on tube expansion.

Consider a length of pump tube as shown in Fig. 11(a). The tube is filled with driver gas at an initial pressure, density, and temperature p_0, ρ_0, and T_0. Once the piston starts moving at a constant velocity U_P equal to the VOD of the explosive used, it will push a PSW in front of it with speed U_s which will bring the driver gas to the shocked state p_s, ρ_s, and T_s. Initially, U_s can be calculated from unsteady shock relations; from there the shocked state can be calculated from normal shock relations.

The flow behind the PSW is subsonic relative to the PSW, which means that changes in pressure and velocity can be communicated through the flow and to the PSW. Thus, it is assumed that the shocked driver gas pressure is uniform. The fact that the tube is expanding will be communicated to the PSW through rarefaction waves, which will slow it down; therefore, U_s becomes a function of time. A lower PSW velocity means a lower pressure ratio across the PSW, and therefore a decrease in pressure of the shocked driver gas.

After some time Δt, the PSW and the piston will be separated by some standoff distance $L_s(t)$, as shown in Fig. 11(a). From the piston-fixed reference frame, the PSW moves away from the piston at a velocity of $\dot{L}_s(t)$. The velocity of the PSW in the laboratory reference frame is then given by $U_s = \dot{L}_s(t) + U_P$.

The mass of driver gas swallowed by the shock at this time is given by:

$$m_{swallowed} = (U_P t + L_s)\rho_o \pi r_0^2,$$

and the mass of shocked driver gas between the piston and the PSW is given by:

$$m_{shocked} = \int_0^{L_s(t)} \rho_s \pi r^2 dx,$$

where r is the pump tube radius and x is in the axial direction of the pump tube. These two masses are identical. Equating and differentiating both sides, the following expression can be obtained, after an application of the Leibniz rule:

$$\left(U_P + \dot{L}_s\right)\rho_o \pi r_0^2 = \int_0^{L_s(t)} \left(\dot{\rho}_s \pi r^2 + 2\rho_s \pi r \dot{r}\right) dx + \rho_s \pi r_0^2 \dot{L}_s(t).$$

The shocked density can be considered constant and in the hypersonic limit is given by:

$$\rho_s = \rho_0 \frac{\gamma + 1}{\gamma - 1}.$$

In this case, $\dot{\rho}_s$ becomes 0.

Simplifying and solving the above equation for $\dot{L}_s(t)$ the following expression is obtained:

$$\dot{L}_s(t) = \frac{U_P - 2(\rho_s/\rho_0)\left(1/r_0^2\right)\int_0^{L_s(t)} r\dot{r}dx}{(\rho_s/\rho_0) - 1}. \tag{4}$$

With this expression, it is possible to solve for the rate of change of the standoff distance $\dot{L}_s(t)$ at a certain point in time if the pump tube radius r and wall speed $\dot{r}$ along the tube between the piston and the PSW are known at that point in time. These values can be obtained from the expanding tube model described above.

The calculation is initialized with an ideal shock which is allowed to travel down the pump tube for a time Δt, over which shock properties are assumed to remain constant. The standoff distance at this time is:

$$L_s(t) = (\Delta t)(U_s - U_P).$$

Over this distance, the expanding tube model is used to evaluate the values of r and $\dot{r}$ at several points, or slices, along the pump tube length, each slice having been exposed to PSW pressure for a time varying between 0 μs (for the slice at the PSW) up to Δt (for the slice at the piston). See Fig. 11(b). Using the obtained discretized radius and tube wall velocity profiles, it is possible to evaluate the integral in Eq. (4), obtain a new value for $\dot{L}_s(t)$ and update the PSW velocity and PSW pressure.

The solution is then advanced by Δt. The new value of standoff is calculated according to:

$$L_s(t + \Delta t) = L_s(t) + \Delta t \dot{L}_s(t).$$

The piston moves forward by a distance $U_P \Delta t$. From the piston-fixed reference frame, the pump tube wall is translated backward by the same amount. Points on the tube profile which are translated behind the piston are discarded, but the points which remain in front of the piston are retained and subjected to the new PSW pressure. The remainder of the length of the pump tube between the piston and the PSW is divided into equally spaced slices. Refer to Fig. 11(c). The process is then repeated, updating the shock properties at each Δt.

For the first few iterations, all slices will be discarded. However, once the standoff distance has grown beyond $U_P \Delta t$, some slices will be retained, and the total number of slices will grow with each iteration. For the pump tube configurations examined, the solution converged when using a Δt of 0.1 μs. With this Δt, initializing the calculation with only 2 slices is enough for the solution to converge.

2. Calculated standoffs and shock velocities

As explained in Sec. IV.B, while in experiments the measurements were made 115 inner tube diameters after the initial collapse point, the calculated values were taken after the PSW had traveled 105 diameters to compensate for the shock formation distance. However, taking the values at either 105 diameters or 115 diameters does not significantly change the results.

Jetting may be responsible for an initial increase in PSW velocity and standoff distance. Such a jet can travel up to twice the VOD of the explosive.[25,26] Therefore, in an attempt to set bounds for the problem, calculations were also done where the PSW velocity was initialized at twice the VOD of the explosive ($U_{s\ initial} = 2U_P$).

For the tamped pump tube series, the recorded VOD was observed to increase with fill pressure due to precompression of the explosive by the expanding pump tube; therefore the VODs used in this case were the ones calculated by Cheetah. The recorded VODs could also have been used; the difference between the results using either value is small.

The calculated standoff distance and PSW velocity versus fill pressure for all three experiment series are shown in Figs. 5 and 6. The calculated standoff curves for each experiment series follow the trends of the measured standoffs quite well and the experimental data for each series lies between both calculated curves for all pressures except the very highest fill pressure used, 100 atm. Since the model uses a constant virtual piston velocity, it cannot be used to reliably predict pump tube behavior at high initial pressures (above 50 atm), where it is suspected that the virtual piston trajectory is discontinuous due to bursting. Nonetheless, agreement is good below 70 atm initial pressure. These results clearly show that the main mechanism for loss of PSW velocity and standoff distance is the radial expansion of the pump tube from the high shocked driver gas pressure. Measured standoff and PSW velocities for the tamped series lie closer to the calculated curves using $U_{s\ initial} = 2U_P$, whereas those for the untamped series lie closer to the curves using $U_{s\ initial}$ = ideal curves, suggesting that jetting is more important in tamped pump tubes. This is reasonable since the inner collapse angle is larger for tamped pump tubes. For both untamped series, the $U_{s\ initial} = 2U_P$ and $U_{s\ initial}$ = ideal curves quickly converge to the same value, which shows that the rapid expansion of untamped pump tubes quickly attenuates the PSW to a point where the effects of initial jetting are no longer visible from the velocity data. However, these

effects are discernible in the standoff data: the increase in PSW velocity imparted by the jet at early times results in an initial rapid increase in standoff, which is why the measured standoff is above the $U_{s\ initial}$ = ideal standoff curve whereas the measured PSW velocity is close to or below the corresponding calculated velocity curve.

It is interesting to note that pump tubes rarely burst according to these model predictions. The faster expansion of the pump tube at higher pressures is compensated by a faster drop in PSW velocity, leading to standoff distances short enough for the pump tube radius to remain below 30% elongation before it is collapsed by the detonation.

C. Failure to pinch

The virtual piston is subjected to shocked driver gas pressure. It is possible for this pressure to be high enough to prevent the pump tube from collapsing onto its axis and forming a complete seal. This would lead to loss of driver gas from the central hole in the virtual piston. Menikoff *et al.*[8] showed that this leaky virtual piston behaves as a nozzle and that the resulting flow can be described by the one-dimensional duct flow equations. This scenario can still drive a PSW, although at a velocity less than the ideal shock driven by a perfect piston, provided the flow is choked at the throat of the imploded region. Eventually, due to loss of driver gas and expansion of the tube walls, the system may reach equilibrium where the PSW travels at the same velocity as the detonation, either ahead of the detonation or within the imploding region.

Several studies have been made on the collapse of cylindrical steel shells. Kinelovskii developed an analytical model to describe the motion of the inner and outer wall surfaces of a tube being collapsed by both infinite[27] and thin[28] layers of explosive, valid up until the point where the inner radius of the tube reaches 20–30% of its initial value. Ivanov *et al.*[29] observed that perturbations in the detonation front cause initial prescribed perturbations on the inner surface of the pump tube. Perturbations on the outer tube wall grow without bound during collapse while waves of finite amplitude develop on the inner wall. Such perturbations were modeled with relative success by Serikov.[30] Ivanov *et al.*[31] noted that the shear strength of the shell material has a substantial stabilizing effect on the development of the perturbations and that there is a minimum tube thickness $\delta^* = \tau/r$ required for stable collapse, where τ is the thickness of the tube and r is the outer radius of the tube. For steel, δ^* has to be larger than 10% for stable implosion.

For the present study, the goal is to completely collapse the pump tube so as to generate long columns of high-pressure gas. The findings above were taken into account when designing the pump tube, mainly for material selection and tube wall thickness, however in the present study a simpler method is sufficient to describe the virtual piston.

Consider a cross-sectional slice of the pump tube which has just been overtaken by the detonation wave. On the outside it is exposed to the detonation pressure of the explosive, on the inside it is exposed to shocked driver gas pressure. Here material strength and the effect of cylindrical geometry are neglected. The tube wall is imparted a kinetic energy per unit area of $(1/2)\rho_{tube}\tau U_{tube}^2$, where U_{tube} is the velocity imparted to the tube wall by the detonation products. As the tube is collapsing, the driver gas inside does work per unit area; if the tube is completely collapsed, this term is equal to $p_{internal}r_0$. As the PSW gets further ahead of the virtual piston, pump tube expansion will gradually decrease the shocked gas pressure, increase the radius of the pump tube, and impart an initial outward velocity to the tube wall; however for a first order approximation these effects can be ignored. For the pump tube wall to just reach the central axis, conservation of energy gives $\frac{1}{2}\rho_{tube}\tau U_{tube}^2 = p_{internal}r_0$. Solving for U_{tube} the following is obtained:

$$U_{tube} = \sqrt{\frac{2p_{internal}r_0}{\rho_{tube}\tau}}.$$

This is the minimum velocity which the explosive needs to impart the pump tube wall so that it just reaches the central axis. However, the time it takes the tube wall to reach the center and the resulting aspect ratio (AR) of the virtual piston, defined as the virtual piston length on the initial pump tube diameter, need to be considered. Since the acceleration of the tube wall due to internal pressure, a, is constant, the time needed to reach the center is given by:

$$t_{pinch} = \frac{U_{tube}}{a} = \frac{U_{tube}}{p_{internal}/(\rho_{tube}\tau)},$$

and the AR is given by:

$$AR = \frac{U_P t_{pinch}}{r_0}.$$

The values of AR obtained by simply imposing a velocity large enough so that the pump tube wall just reaches the central axis are not realistic. From a design point of view, it is better to impose a certain AR and then work out the pump tube wall velocity needed.

The Gurney velocity approximation[25] was used to determine the inward velocity imparted to the pump tube wall by the detonating layer of explosive surrounding it. The open-faced sandwich equation was used for untamped pump tubes:

$$U_{tube} = \sqrt{2E}\left[\frac{\left(1+2\frac{M}{C}\right)^3+1}{6\left(1+\frac{M}{C}\right)} + \frac{M}{C}\right]^{-\frac{1}{2}},$$

and the asymmetric sandwich formula was used for tamped pump tubes:

$$U_{tube} = \sqrt{2E}\left[\frac{1+A^3}{3(1+A)} + \frac{N}{C}A^2 + \frac{M}{C}\right]^{-\frac{1}{2}},$$

where

$$A = \frac{1+2(M/C)}{1+2(N/C)}.$$

Here, $\sqrt{2E}$ is called the Gurney characteristic velocity and is specific to the explosive used, M/C is the metal-charge mass

ratio for the pump tube and N/C is the metal-charge mass ratio for the tamper. The initial tube wall velocities were calculated to be 1.11 km/s for the 0.64 cm untamped series, 1.53 km/s for the 1.27 cm tamped series, and 1.35 km/s for the 1.27 cm untamped series.

Improvements on the Gurney formula have been made to account for cylindrical geometries. Models from Hennequin[32] and Chou *et al.*[33] give an expression similar to Gurney which includes an extra integral. Hirsh[34] simplified the Chou formula but the results include a scaling parameter which is not defined and needs to be guessed or experimentally calibrated. The Chanteret[35] formula can be used in a straightforward manner, but it does not appreciably deviate from the original Gurney formula except for extremes of M/C. Carleone and Stefan[36] also developed an analytical model for thin collapsing shells including the effects of spinning and material strength. They concluded that spin and, more importantly for the present case, material strength were significant and may greatly reduce the final collapse velocity. Nonetheless, the method described here is only meant as a simple first order approximation and the extra complications associated with these modified formulas were found to not affect the qualitative nature of the results.

The results of this model predict that complete pinch of the pump tubes should have occurred with an AR below 6 for all tests described in Sec. II. A precursor was observed in all experiments, thus results are consistent with predictions. However, in some experiments not reported here, a virtual piston calculated to have an AR above 7 was not able to drive a PSW. Thus it is recommended to have an AR as small as possible, preferably below 6.

D. Parameter maps

Pump tube operation is influenced by a large number of different parameters; as a result there are many reasons the tube may fail to operate as intended. The expanding tube model presented above is a useful tool to predict pump tube behavior for any given configuration. By fixing some parameters and allowing others to vary, it is possible to generate conceptual parametric "maps" and define regions of expected behavior.

Figure 12 shows the effect of varying initial fill pressure for different explosive layer thicknesses for given pump tube dimensions. In regions 1 and 2 of this figure, a precursor can be driven without bursting the tube either without a tamper (region 1) or at even higher initial pressure (region 2) with a tamper. In regions 3 and 4, the tube bursts before the arrival of the detonation due to the tamper failing mechanically (region 3) or the tamper not being able to communicate with the pump tube due to the explosive layer being too thick (region 4). In regions 5 and 6, the tube is not imploded with a sufficiently small aspect ratio to drive a precursor effectively either without tamper (region 5) or with a tamper (region 6). Thus, the high-pressure operation (80 atm) that permits a precursor occurs with a thin layer of explosive (2 mm) using a heavy tamper. This figure thus identifies the parameters that influence design. Increasing the explosive layer thickness is beneficial in the absence of a tamper; a thinner layer is better when using a tamper since the effect of the outer boundary will be felt at an earlier time. When using a tamper, it is also possible to use much higher initial fill pressures, and it is easier to completely collapse the pump tube.

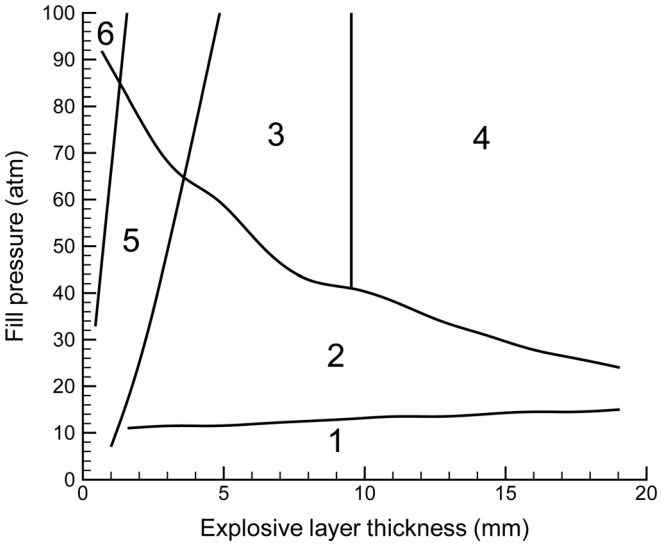

FIG. 12. Parameter map showing regions of expected behavior when varying the initial fill pressure and explosive layer thickness for a 1 m long, 1.27 cm OD, 1.09 cm ID pump tube. In the untamped case, the outer tube is a 3.18 cm thick PETG tube, for the tamped case it is a 1.27 cm thick steel tube. (1) Untamped pump tube does not fail, (2) Tamped pump tube does not fail, (3) tamper ineffective (tamper fails), (4) tamper ineffective (tamper too far from pump tube), (5) untamped pump tube does not collapse completely, and (6) tamped pump tube does not collapse completely.

VI. CONCLUSIONS

The simple, analytical model developed in this study is able to reproduce the observed shock dynamics of an explosively driven imploding pump tube. This model permits the construction of a parameter map which identifies the set of parameters for which a long-duration, high-velocity precursor shock wave can be generated. The use of this model has contributed to the optimization of the pump tube design for use in a hypervelocity launcher that has demonstrated a muzzle velocity of 7.3 km/s with a 10 g projectile, which is comparable to the best performance of conventional light gas guns.[37] This model can also be extended to investigate an advanced hypervelocity launcher concept where explosives are continued along the launch tube to maintain a high driving pressure on the projectile.

In addition to the nonideal effects investigated in this study (expansion of the pump tube, failure of the explosive to pinch), other effects are present in the operation of an implosion driven pump tube. The high shock temperatures generated (6200 K incident shock, 14,500 K reflected shock) will result in melting and vaporization (ablation) of the pump tube wall due to both convective and radiative heat transfer.[15–19] The entrainment of tube wall material (iron, etc.) into the gas will result in an increase in the effective molecular weight, which is expected to have a significant deleterious impact on performance of the shock-heated gas as a gas-gun propellant. The stability of the explosive pinch and the possibility of gas leaking past the pinch due to

instability or boundary layer effects may also be a phenomenon limiting how fast the precursor shock may be driven. These effects should be considered in future studies.

ACKNOWLEDGMENTS

The authors would like to thank Patrick Bachelor for both his help in conducting experiments and his frequent and useful input relative to this study. The authors would also like to thank Gary Savard, John Boisvert, and Raymond Lemay for their assistance in machining parts needed for the experiments as well as Justin Huneault and Matthew Serge for their constructive feedback regarding this study. This project was supported by the Canadian Space Agency, CSA Contract No. 9F028-064201/A, and the Defense Research and Development Canada, DRDC Contract No. W7701-82047.

[1]W. S. Koski, F. A. Lucy, R. G. Shreffler, and F. J. Willig, J. Appl. Phys. **23**,1300 (1952).
[2]I. I. Glass, Prog. Aerosp. Sci. **13**, 223 (1972).
[3]H. F. Waldron, E. T. Moore Jr., G. B. Steel, and C. S. Godfrey, in *AIAA 5th Aerospace Sciences Meeting*, New York, 1967.
[4]J. K. Crosby and S. Gill, "Feasibility study of an explosive gun," NASA CR-709, 1967.
[5]E. T. Moore, "Explosive hypervelocity launchers," NASA CR-982, 1968.
[6]J. D. Watson, "High-velocity explosively driven guns," NASA CR-1533, 1970.
[7]D. W. Baum, "Development of explosively driven launcher for meteoroid studies," NASA CR-2143, 1973.
[8]R. Menikoff, K. S. Lackner, N. L. Johnson, S. A. Colgate, and J. M. Hyman, Phys. Fluids A **3**, 201 (1991).
[9]V. Tanguay and A. J. Higgins, J. Appl. Phys. **95**, 6159 (2004).
[10]V. Tanguay and A. J. Higgins, J. Appl. Phys. **96**, 4894 (2004).
[11]C. H. Johansson and A. Persson, *Detonics of High Explosives* (Academic Press, London, 1970).
[12]H. Mirels, AIAA J. **2**, 84 (1964).
[13]S. P. Gill and R. C. Goettelman, "Implosively accelerated shock tube driver," NASA CR-950, 1967.
[14]S. P. Gill, Phys. Fluids **12**, I-88 (1969).
[15]H. D. Glenn and B. K. Crowley, J. Appl. Phys. **42**, 2099 (1971).
[16]N. I. Matyushkin and Y. A. Trishin, J. Appl. Mech. Tech. Phys. **3**, 142 (1977).
[17]R. Schreffler and R. Christian, J. Appl. Phys. **25**, 324 (1954).
[18]S. D. Savrov and I. M. Ageev, High Temp. **6**, 1257 (1980).
[19]C. R. Jones and W. C. Davis, "Optical properties of explosive-driven shock waves in noble gases," LA-9475-MS, 1982.
[20]L. E. Fried, W. M. Howard, and P. C. Souers, "Cheetah 2.0 Users' Manual," URCL-MA-117541 Rev. 5, Lawrence Livermore National Laboratory, 1998.
[21]J. J. Lee, J. Jiang, K. H. Choong, and J. H. S. Lee, Shock Compression Condens. Matter–1999, 797 (2000).
[22]M. Brouillette, J.-P. Dionne, M. Radulescu, J. Jiang, J. J. Lee, and J. H. S. Lee, in *Proc. 21st International Symposium on Shock Waves,* Queensland, Australia, 1997.
[23]J. M. Winey, G. E. Duvall, M. D. Knudson, and Y. M. Gupta, J. Chem. Phys. **113**, 7492 (2000).
[24]G. R. Johnson and W. H. Cook, in *Proc. of the 7th International Symposium on Ballistics*, The Hague, Netherlands, 1983, pp. 541–547.
[25]W. P. Walters and J. A. Zukas, *Fundamentals of Shaped Charges* (Wiley, New York, 1989), pp. 45–63, 72–77.
[26]G. Birkhoff, D. P. MacDougall, E. M. Pugh, and G. Taylor, J. Appl. Phys. **19**, 563 (1948).
[27]S. A. Kinelovskii, Combust. Explos. Shock Waves **16**, 73 (1980).
[28]S. A. Kinelovskii, Combust. Explos. Shock Waves **10**, 110 (1983).
[29]A. G. Ivanov, Y. D. Lavrovskii, and V. A. Ogorodnikov, J. Appl. Mech. Tech. Phys. **33**,723 (1992).
[30]S. V. Serikov, J. Appl. Mech. Tech. Phys. **25**, 142 (1984).
[31]A. G. Ivanov, V. A. Ogorodnikov, and E. S. Tyun'kin, J. Appl. Mech. Tech. Phys. **33**, 871 (1992).
[32]E. M. Hennequin, in *Proc. 7th International Symposium on Ballistics*, The Hague, Netherlands, 1983.
[33]P. C. Chou, J. Carleone, E. Hirsch, W. J. Flis, and R. D. Ciccarelli, in *Proc. 6th International Symposium on Ballistics*, Orlando, FL, 1981, pp. 27–29.
[34]E. Hirsch, Propellants Explos. Pyrotech. **11**, 6 (1986).
[35]P. Y. Chanteret, in *Proc. 7th International Symposium on Ballistics*, The Hague, Netherlands, 1983.
[36]J. Carleone and R. Stefan, Propellants Explos. Pyrotech. **18**, 299 (1993).
[37]V. Tanguay, D. Szirti, J. Loiseau and A. J. Higgins, in *Proc. 11th Hypervelocity Impact Symposium*, Freiberg, Germany, 2010.